ANALYSIS OF THE INTERVERTEBRAL DISCS ADJACENT TO INTERBODY FUSION USING A MULTIBODY AND FINITE ELEMENT CO-SIMULATION

Nuno Miguel Barroso Monteiro
Instituto Superior Técnico
Av. Rovisco Pais, P-1049-001 Lisboa
nuno.barroso.monteiro@gmail.com

Abstract

This work describes a novel methodology for the dynamic and structural analysis of complex (bio)mechanical systems that joins both multibody dynamics and finite element domains, in a synergetic way, through a co-simulation procedure that takes benefit of the advantages of each numerical formulation. To accomplish this goal, a co-simulation module is developed based on the gluing algorithm X-X, which is the key element responsible for the management of the information flux between the two software packages (each using its own mathematical formulation and code). The X-X algorithm uses for each co-simulated structure a pair of reference points whose kinematics are solved by the multibody module and prescribed, as initial data, to the finite element counterpart. The finite element module, by its turn, solves the structural problem imposed by the prescribed kinematics, calculates the resulting generalized loads applied over the reference points and return these loads back to the multibody module that uses them to solve the dynamic problem and to calculate new reference kinematics to prescribe to the finite element module in the next time step. The proposed method is applied to study the spine (cervical and lumbar) dynamics in a pathologic situation, in which an intersomatic fusion between one or more spine levels is simulated. Taking into account the proposed simulation scenario, three major components are developed and included in the model: the spine multibody model (being the cervical model an adaptation of the de Jager's cervical model and the lumbar spine obtained from measurements retrieved or/and adapted from the literature) that includes the rigid vertebrae, the facet joints' and spinous processes' contacts, ligaments and the finite element models of the intervertebral discs and of the fixation plate. The proposed model is simulated for flexion and extension movements in a forward dynamics perspective.

Keywords: Co-simulation, Multibody Systems, Finite Element, Spine, Intervertebral Disc, Fixation Plate, Forward Dynamics.

1. Introduction

The vertebral column not only allows for a wide range of movements, including lateral flexion, left and right rotation and flexion of the torso, but it also encloses and protects the spinal cord, supports the head, and serves as a point of attachment for the ribs and the muscles of the back. Adjacent vertebrae (from C2 to the sacrum) are interconnected by intervertebral discs (IVD), which are slightly movable joints that allow 6 degrees-of-freedom movements and absorb vertical shocks [1]. Besides each disc grants a limited motion to the motion segment, the set of the 23 intervertebral discs provide the spine with great flexibility and motion.

The intervertebral disc is an inhomogeneous, anisotropic, porous, nonlinearly viscoelastic structure [2, 3] that, simultaneously with the articular facets, has an important role in the spine biomechanics, namely, in transmitting loads (between 500 and 5600 N for normal discs) between adjacent vertebral bodies [4,5], in supporting and attenuate compression loads [3,6], as well as, in the spine mobility [5].

In each disc it is possible to distinguish three regions: a peripheral region, the annulus fibrosus, consisting of quasi-concentric lamellae of fibrocartilage; a soft and highly elastic posterocentral region, the nucleus pulposus; and an upper and lower cartilage (hyaline cartilage towards its vertebral surface and fibrocartilage towards its discal surface), connecting the annulus and nucleus to the vertebral core [7], the endplates.

The most common fractures in the intervertebral disc occur in the endplate and in the annulus, which tend to appear with age or degeneration or due to an applied load associated with a non-physiological motion. These fractures translate in failure or in the appearance of fissures, which determines the loss of integrity of the annulus and through which the nucleus pulposus material passes to the fibers of the annulus and to the spinal canal. The process of degeneration often leads to herniation, which occurs when the nuclear material is emitted and compresses the medulla or nerve roots [8]. Notice that irreversible spinal coord injury becomes very probable when the compression exceeds ⅓ of its normal diameter [9]. Furthermore, the decreased height tends to increase the loads exerted over the posterior elements, namely the articular facets [10].

Intersomatic fusion is required when it is necessary to reestablish the intervertebral disc function and conservative treatment not produces the intended results. This surgical procedure is characterized by the union of two or more adjacent vertebrae through replacement of the pathologic disc by an artificial surrogate or a bone graft (autograft, from the own's

patient bone, or allograft, bone from a donor different of the receiver, of the same species), which provides a substrate for reconstruction of the vertebral column by bone fusion of the adjacent vertebrae [11]. This surgical procedure, also known as intervertebral body fusion, was firstly described by Robinson and Smith in 1955 [12] for the treatment of disc degeneration with nerve root compression and its goal is to support the spine, maintain correction and alleviate pain by diminishing movement [13,14].

In a great number of cases, the stresses experienced by these materials are high and, consequently, there is a real danger of being expelled or crushed. To avoid and prevent this from happening, fixation devices are incorporated when an intersomatic fusion takes place. Nonetheless, the fixation devices has some well known disadvantages due to the Young modulus of their materials, usually from titanium alloys (E = 115 GPa), which are greater than that of the bone (E = 12 GPa, for cortical bone). This result in a phenomenon denominated of stress shielding and consists in a diminished vertebral bone density due to a reduction of the normal stress supported by the bone, which induces a non-equilibrated activity of osteoblasts (responsible for bone formation) and osteoclasts cells (responsible for bone resorption). As such, to decide which type of implant and the materials that compose the implant two factors have to be taken into account: the implant's efficiency in stabilizing the region where it is inserted by evaluating the region mobility, and the ability of the implant to bypass and withstand the forces by evaluating the stress distribution in the different parts of the implant [15].

Despite this technique has been considered as a common routine to re-establish the stability of the spine in case of pathology, it has disadvantages, namely, on the adjacent structures. There are several studies that report increases in stress up to 96% in the adjacent levels for all loading situations leading to accelerated degeneration and spinal refusion with spine fusion [14], and alterations on the motion segments adjacent to interbody fusion (41% of the patients followed) being necessary secondary operations in about 20% of the patients followed [16]. Nonetheless, other studies support that fusion and plating do not increase motion or intradiscal pressure in adjacent levels [17]. As such, to study the influence of an intersomatic fusion on the adjacent IVDs, a co-simulation module has been developed to link the multibody system dynamics (MSD) with the finite element (FE) softwares.

The conjunction of the multibody system dynamics and finite element is scarcely applied to analyze the multibody dynamics of flexible bodies. Nonetheless, as a consequence of new integration algorithms [18] and the advent of computers, the future of these two domains is to decrease the gap between them. Hence, the relevance and importance of its employment has increased, namely in applications to the railway industry, for example in modelling a catenary pantograph contact [19].

In spine biomechanics, these two computational domains have been used independently and prove to be a good choice when the goal is to obtain the kinematics and loads that the spine carries (MSD), or the stress distribution in each spine internal structure (FE). Having the scientific community played an important role in developing the spine models, which have evolved greatly since in 1957 an analytic model to analyze the spine was described [20], that allows simulating realistically its behaviour for the most varied loading situations in order to understand the load transfer and the importance of each of its component to the spine stability and function, as well as its response in accidents and injuries [15,21,22,23,24]. However, the combination between the two methods is barely applied, and no studies in this area have been perceived of using a real integration and simultaneous execution of the two formulations. The studies that use both methods are used to complement the information provided by each one of the numeric methods by prescribing a load history (from the MSD) to a specific interface of the FEMs in isolated analyses [25,26,27].

In the current work, a co-simulation between the two numerical methods is described, which benefits from the advantages of each method to outcome and complement the disadvantages of the other, establishing a real synergetic link between the MSD and FE.

The objectives of this work are to develop an efficient and robust method for the co-simulation between the multibody system dynamics and finite element formulations, allowing the flux information management between the two domains, and assemble a detailed and validated biomechanical model of the cervical and lumbar spine regions, with the aim of comparing the stress distribution in the intervertebral discs before and after the intersomatic fusion, and also the movement restriction of the spine. With this purpose, a multibody model of the two spine regions with a detailed vertebral geometry, and complex finite element models of the intervertebral discs and their surrogates, as well as, a FEM of a fixation plate are developed.

2. Methods and Model

The computational methods and models described hereafter are implemented and simulated in the FORTRAN code/program APOLLO [28], which is a general purpose MSD simulator that uses a multibody formulation with natural, or fully-Cartesian, coordinates to perform forward (or inverse) dynamic analyses. In APOLLO, several modules are implemented and improved, which include the ligaments, the contact pairs and the six degree of freedom (DOF) bushing elements [29]. The finite element models of the IVDs, their surrogates and of the fixation plate are modeled using the ABAQUS software package. The co-simulation module core is incorporated into the APOLLO code while the file management and linkage with ABAQUS is developed in Python language.

2.1 The Spine Multibody Model

The spine regions developed in the current work are a combination of an adaptation of the de Jager's cervical model and a lumbar model developed with dimensions either retrieved from the literature or computed based

upon the literature values. The cervical (lumbar) spine model consists of 9 (6) rigid bodies defining the head and vertebrae C1-T1 (L1-S1), with 49 (35) ligaments, and 23 (15) contacts comprising the articular facets and the contact between the spinous processes. In order to simplify the spine model, it is assumed that the spine is symmetric relatively to the sagittal plan.

The geometry of the vertebrae is important in the definition of a spine model, since it is to this bony structure that ligaments and muscles attach [30]. As such, a complex representation of the vertebra structure allows assembling a complex spine model as long as the soft tissue's attachment points are known relatively to a local reference frame. The posterior region of the vertebral body is aligned with the z-axis of the local reference frame, being the x-direction defined as a line traversing the vertebral body from its posterior to anterior region and the y-direction defined from its right to its left side. This way a right-handed reference frame is defined, whose origin is located at the posterior mid-height of the vertebral body (Figure 1).

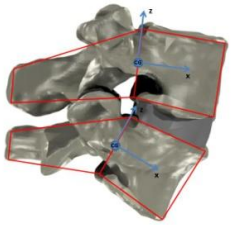

Figure 1 – Representation of the local reference frame associated to a given vertebrae and spine level.

The global coordinates associated to each vertebrae (or local reference frame) are adapted from the work of Stokes et al. [31], Gangnet et al. [32], de Jager [33] and Ferreira [29]. The first two studies are used to define the initial positions and orientations of the lumbar spine while the remainders are used to define the geometrical representation of the cervical spine.

The inertial properties of each body level are computed assuming that they can be lumped into the origin of the respective local reference frame. These body levels represent slices of a given region of the body comprising all hard and soft tissues between two consecutive intervertebral spaces (i.e., containing only one vertebra).

For the cervical spine, these properties are retrieved from Ferreira [29] which adapted the moments of inertia reported by de Jager [33] through the theorem of parallel axes. According to de Jager, the neck is considered a solid cylinder with a total mass of 1.63 kg, which is divided into seven segments whose heights correspond to the displacement between adjacent local reference frames.

On the other hand, the lumbar spine is considered to be divided into five segments and the data used to compute their inertial properties are retrieved from the anthropometric model of the code SOM-LA [34]. The inertial properties are computed by approximating each level to a solid elliptical cylinder with mass M, height L_z, radius L_x and L_y, respectively, using the following equations (assuming that the local reference frame origin coincides to the center of gravity):

$$I_{xx} = \frac{M}{12}\left(3L_y^2 + L_z^2\right) \quad (1)$$

$$I_{yy} = \frac{M}{12}\left(3L_x^2 + L_z^2\right) \quad (2)$$

$$I_{zz} = \frac{M}{4}\left(L_x^2 + L_y^2\right) \quad (3)$$

2.2 Co-Simulation Module

The conjunction between the MSD and FE has been scarcely described and used as an alternative approach to the dynamic analysis of mechanical systems. However, the two methods can be used simultaneously to overcome their disadvantages in a really synergetic link, benefiting of the multibody dynamics formalisms capacity to incorporate other disciplines [35]. The multibody system models have a simpler geometry relatively to the finite element models, since only the points defining the elements geometry and involved in joints or other structures are needed. Furthermore, the material description for the finite element formulation is far more complex than that of the multibody systems. As such, the multibody formulation is faster and less demanding on computational time than finite elements formulation. On the other hand, the MSD define precisely the global and local kinematics of a given (bio)mechanical model. A major drawback of the multibody formulation is that the elements are considered as rigid bodies, which limits its capability to analyze stresses. Consequently, if the goal is to investigate the intrinsic mechanical behavior for a specific set of elements considering the dynamics of the global structure where they are incorporated, the two methods can be merged in order to complement the information from each other and diminish the computational cost for a given analysis.

With the intention of performing a simultaneous execution of the two computational domains (MSD and FE), an independent co-simulation model (Figure 2) is proposed and developed. This model allows linking the two domains using pairs of reference points (RP), through which a bidirectional flux of information is established. Initially, this model [36,37] was used to link the rigid vertebral bodies (MSD) to the flexible intervertebral disc (FE) using only one pair of RP, as illustrated in Figure 2. Presently, an improvement is introduced to obtain a more complex and real deformation of the flexible bodies, so more reference points are used in the interface between the two domains (namely, in the fixation plate model) [38,39]. The linkage module described herein is based on the gluing algorithm denominated by the X-X method (proposed by Wang et al. [18]) and consists in the prescription of the RP kinematics (positions and rotations) by the multibody system software (APOLLO) to the finite element software (ABAQUS), which by its turn returns the structural response of the flexible body (forces and torques). The X-X method is one of the gluing algorithm variants introduced by Wang, Ma and Hulbert that can be used for static, dynamic and multibody dynamic component models of a given (bio)mechanical system, which is more convenient for forward dynamic analysis in order to acknowledge the

load (**T**) necessary to apply to each subsystem for producing a given motion characterized by (**X**).

In each co-simulation model there are only and always two bodies, a constrained Master body and a mobile Slave body, which are defined in the multibody system model. The boundary, sharing common surfaces with the two rigid bodies, has several pair of points, the RP, which are used to define its deformation and are denominated by Master or Slave point according to the body that they belong.

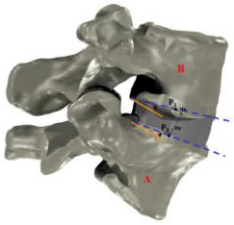

Figure 2 – Co-simulation model.

Considering a pair of reference points of a given co-simulation model, there is a Master point (P_2) according to which the input is given to the finite element software (being constrained in all six DOF), and a Slave point (P_1) that drives the deformation of the model. In order to define the motion of the finite element model, a total of six degrees of freedom have to be prescribed (three translational and three rotational values), according to the Euler's and, the subsequent, Chasles's Theorem that states that the most general movement of a body is a rotation plus a translation.

Assuming the global coordinates of the master and slave points ($\mathbf{r}_{P_2}$ and $\mathbf{r}_{P_1}$ respectively), the translational values (**Δ**) given as input for ABAQUS are given by:

$$\mathbf{\Delta} = \mathbf{A}_A^T\left(\mathbf{r}_{P_1} - \mathbf{r}_{P_2}\right) \tag{4}$$

where $\mathbf{A}_A$ is the transformation matrix of the master body of the co-simulation model.

On the other hand, the rotational values (φ) are obtained from the Euler parameters (**e**) [40]. The Euler parameters are chosen since they allow determining uniquely the rotations that define the body's orientation relatively to a given frame, conversely to the Euler or Bryant angles. In order to compute the parameters' values, a first evaluation for the value of e_0 is performed considering the trace of $\mathbf{A}_{BA}$ (transformation matrix of the slave body relatively to the master body):

$$e_0^2 = \frac{\mathrm{tr}\left(\mathbf{A}_{BA}\right)+1}{4} \tag{5}$$

If the value of e_0 is zero, one of the remaining values of the Euler parameters is necessarily non-zero and can be determined using the diagonal entries of the transformation matrix $\mathbf{A}_{BA}$:

$$e_i^2 = \frac{1+2a_{ik} - tr\left(\mathbf{A}_{BA}\right)}{4} \quad , \quad i=k,\ i=1,2,3 \tag{6}$$

After finding the nonzero parameter, it is necessary to use the non-diagonal entries to define the remaining Euler parameters. In summary, the pathway to determine these parameters is described and detailed in the flowchart presented in Figure 3.

ABAQUS Manuals refer that the rotation values given as input to ABAQUS/CAE are the rotations about the axis of the global coordinate system, or of the axis of another coordinate system associated with the specific degrees of freedom. These rotations, afterwards, are used to obtain the rotation value φ presented in Eq. 7 and the respective axis of rotation **h** defined in Eq. 8 (Figure 4).

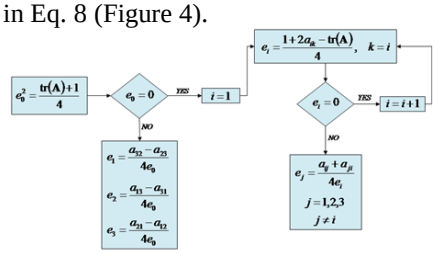

Figure 3 – Fluxogram to define the Euler parameters values.

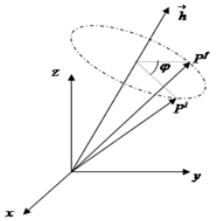

Figure 4 – Representation of a body rotation.

$$\varphi = \sqrt{\varphi_1^2 + \varphi_2^2 + \varphi_3^2} \tag{7}$$

$$h_1 = \frac{\varphi_1}{\varphi}, \quad h_2 = \frac{\varphi_2}{\varphi}, \quad h_3 = \frac{\varphi_3}{\varphi} \tag{8}$$

Comparing this definition (Eq. 7 and Eq. 8) with the Euler parameters (Eq. 5 and Eq. 6) and taking into account the trigonometric properties, the following relation can be inferred:

$$\begin{cases} e_0 = \cos\left(\dfrac{\varphi}{2}\right) \\ \mathbf{e} = \mathbf{h}\sin\left(\dfrac{\varphi}{2}\right) \end{cases} \Rightarrow \begin{cases} \varphi = \cos^{-1}\left(2e_0^2 - 1\right) \\ \varphi_i = \dfrac{2e_i e_0}{\sin(\varphi)}\varphi \end{cases}, i = 1,2,3 \tag{9}$$

With the definition of the translational and rotational values, corresponding to the degrees of freedom of a given body, as well as the time increment between consecutive analysis (velocities and angular velocities are implicitly defined) its motion can be prescribed completely.

The multibody integration method is characterized by a multi-time step depending on the stability of the integrator and the integrator convergence rate in a given analysis. Moreover, the co-simulation module executes a finite element analysis by each step analysis (predictor and corrector) in the multibody integration method, an efficiency procedure is of major importance in reducing the real time analysis. In the current work, a method that improves the co-simulation efficiency based on a linear regression of the finite element data is described. This method assumes that between each analysis step there is a very small variation in the values prescribed to the FEMs, due to the very small time steps. Hence, the output values from the FEMs can be approximated using a weighted linear interpolation or extrapolation of the data in their vicinity.

In order to test the linkage between the two domains, a simple multibody model is developed comprising two rigid bodies and a flexible body defined in finite elements (Figure 5). The finite element model of the cylinder has a Young modulus E of 31,831 MPa and a

Poisson coefficient of zero. The Poisson coefficient is zero in order to avoid deformation in the transversal directions.

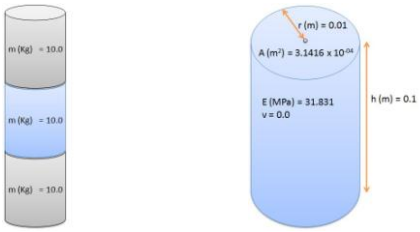

A **B**

Figure 5 – Global multibody test model assembled (**A**) and finite element model of the cylinder (**B**).

This test model is subjected to different loading situations (flexion, torsion, axial and transverse loading) in order to evaluate the cylinder dynamic behavior, namely its displacements and rotations, using the finite element model and an equivalent multibody model. Also, the maximum deformations are compared to the value obtained from the mechanical theory assuming a static situation. Notice that the upper surface of the upper rigid body is constrained in all six DOF in the tests performed and the loads are applied on the lower body. To introduce the dynamical behavior in the structure, the moments of inertia are determined for each body. Comparing the several results, it can be seen that the co-simulation proposed provide good results for all loading situations, not exceeding the maximum error the limit of 5%: 1.6% for displacements in axial loading, 3.44% for rotations in torsion, 0.92% for displacements in flexion, and 4.16% for moments in transverse loading. On other hand, comparing these results with that obtained with bushing elements, it can be seen that for more complex loading situations (flexion and transverse loading) the co-simulation provide better results. Contrarily, the bushing elements provide better results in the other load scenarios (torsion and axial loading), nonetheless, the load error using finite element models not exceeds 0.13%.

2.3 Ligaments and Contacts

Ligaments and facet joints have great importance on the overall spine stability as they are able to absorb energy during normal and traumatic situations [41]. Moreover, the ligaments are important in resisting flexion rotation and posterior shear, while facets are responsible for resisting large extension rotation and anterior shear [42]. Ligaments work in their toe-in region (when spine is under its physiological range of motion), which is characterized by a relatively high deformation in response to a small applied load, conferring the spine with its neutral zone [43,44]. On the other hand, the articular facets, like the intervertebral disc, are the more important load bearing structures of the spine [45] carrying about 18% of the total compressive load on a given motion segment, reaching to 33% depending upon the spine posture [3].

Ligaments are viscoelastic structures composed mainly of collagen and elastin that connect two or more bones together and are important in joint stabilization, by limiting its possible movements, in maintaining the correct bone and joint geometry [46], and in absorbing energy during trauma [41], by developing strain and stress in the ligament. Ligaments exhibit a characteristic mechanical behavior comprising three distinct regions: the toe-in region (small load determines a large deformation; the collagen fibers are straightened up), the linear region (collagen fibers start to deform), and the failure region (ligament stiffness starts to decrease).

Ligaments are modeled as nonlinear viscoelastic structures, being their elastic behavior described using the approach proposed in the knee model developed by Wisman [47], while their viscous properties (namely the hysteretic behavior) are modeled using a strain rate dependent force component weighted by a coefficient C when the ligament is in the loading phase cycle as reported in van der Horst's model [48]. Therefore, considering that ligaments are structures that only produce force when tensioned, the total force, F_T, exerted by a ligament is given by:

$$F_T = \begin{cases} F_E & , \quad \varepsilon > 0 \wedge \dot{\varepsilon} \leq 0 \\ F_E\left(1 + C\dot{\varepsilon}\right) & , \quad \varepsilon > 0 \wedge \dot{\varepsilon} > 0 \\ 0 & , \quad \varepsilon \leq 0 \end{cases} \tag{10}$$

where F_E is the elastic force module, defined as:

$$F_E = \begin{cases} \dfrac{K\, L_0 \varepsilon^2}{2\, \varepsilon_B} & , \quad 0 < \varepsilon < \varepsilon_B \\ K\, L_0 \left(\varepsilon - \varepsilon_B / 2\right) & , \quad \varepsilon \geq \varepsilon_B \end{cases} \tag{11}$$

In the previous equation ε_B is the transition strain value between the toe-in and the linear region, K is the stiffness of the ligament (in Newton per meter), L_0 is the resting length of the ligament, ε is the ligament strain (Eq. 12) for a given length (L) and $\dot{\varepsilon}$ is the corresponding strain rate (Eq. 13):

$$\varepsilon = \frac{L - L_0}{L_0} \tag{12}$$

$$\dot{\varepsilon} = \frac{d\varepsilon}{dt} = \frac{\dot{L}}{L_0} \tag{13}$$

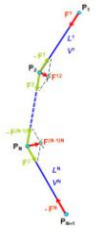

Figure 6 – Ligament model with N segments, with representation of the force direction applied along the ligament.

The developed ligament model considers the use multiple points in the definition of the ligament path, as represented in Figure 6. This allows a more accurate description of the force exerted along the ligament, particularly in what refers the direction according to which this force is applied. The position of these viapoints is expressed in the local coordinates of the rigid body to which they wrap around.

Considering a ligament defined by N segments, the total force exerted when it is subjected to a tensile load depends on its length and its lengthening velocity as a whole. Therefore, the ligament total length (L) is given by the sum of each segment length, i.e., the norm of the

difference between the position vectors of the two points that define the segment:

$$L = \sum_{i=1}^{N} L^i = \sum_{i=1}^{N} \left\| \mathbf{r}_{P_{i+1}} - \mathbf{r}_{P_i} \right\| \quad (14)$$

Likewise, the ligament total lengthening velocity ($\dot{L}$) is defined as the sum of the projection of the relative velocity between the points that define each segment on the unitary vector of the ligament segment, $\mathbf{u}^i$. Analytically $\dot{L}$ and $\mathbf{u}^i$ are respectively defined as:

$$\dot{L} = \sum_{i=1}^{N} \dot{L}^i = \sum_{i=1}^{N} \left(\dot{\mathbf{r}}_{P_{i+1}} - \dot{\mathbf{r}}_{P_i} \right)^T \mathbf{u}^i \quad (15)$$

$$\mathbf{u}^i = \frac{\mathbf{r}_{P_{i+1}} - \mathbf{r}_{P_i}}{\left\| \mathbf{r}_{P_{i+1}} - \mathbf{r}_{P_i} \right\|} \quad (16)$$

After obtaining the force module and the unitary vectors of the ligament segments, these are applied to compute the force exerted by the ligament in all of its points. As it can be seen from Figure 6, for isolated points (that only have the contribution of one segment) the ligament force is given by Eq. 17, while for shared points (that have the contribution of two segments) the ligament force is given by Eq. 18.

$$\mathbf{F}^i = F_T \, \mathbf{u}^i \quad (17)$$

$$\mathbf{F}^i = F_T \left(\mathbf{u}^{i+1} - \mathbf{u}^i \right) \quad (18)$$

In the current model, the force produced in the failure region is considered constant and equal to the maximum force exerted by the ligament in the linear region. Notice that pretension (F_{PT}) can be included into the ligament by reevaluating its length (L_{PT}) using:

$$L_{PT} = \left(L_0 + \frac{\varepsilon_B F_{PT}}{K L_0} \right) - \sqrt{\frac{\varepsilon_B F_{PT}}{K L_0} \left(2 L_0 + \frac{\varepsilon_B F_{PT}}{K L_0} \right)} \quad (19)$$

Due to the importance of the articular facet and spinous process contacts in the spine biomechanics, and also of the upper cervical and head contacts, namely between the atlas, axis and occipital condyles, a contact model based on the nonlinear Kelvin-Voigt contact model is developed [49, 28], which is based on the nonlinear Hertz law [50]. According to this model the force module, F_C, arising from a contact between two structures is given by:

$$F_C = K \delta^n + D \dot{\delta} \quad (20)$$

where K is the relative stiffness between the surfaces in contact, D is the relative hysteretic damping, n is the nonlinearity parameter, δ is the pseudo-penetration and $\dot{\delta}$ is the pseudo-velocity. The relative stiffness and hysteretic damping depend on the geometry and material properties of the surfaces in contact. As contact is considered to be established between a sphere (i) and a plan (j), these two properties of the contact model are given by Eq. 21 and Eq. 22, respectively:

$$K = \frac{0.424 \sqrt{r}}{\left(\frac{1 - \nu_i^2}{\pi E_i} + \frac{1 - \nu_j^2}{\pi E_j} \right)} \quad (21)$$

$$D = \frac{3K\left(1 - e^2\right)}{4 \dot{\delta}^{(-)}} \delta^n \quad (22)$$

where r is the sphere radius, v is the Poisson coefficient, E is the Young modulus, e is the restitution coefficient and $\dot{\delta}^{(-)}$ is the pseudo-velocity before impact. Notice that, contrarily, to the relative stiffness, the relative hysteretic damping varies with time, according to the values of the pseudo-penetration and the pseudo-velocity before impact.

The contact force is applied only when contact between the surfaces occurs. This is determined using two reference points to describe the spatial position of the plan (complemented also with its normal $\mathbf{n}_P$, that is used to define its spatial orientation) and sphere, and two other parameters (the sphere radius r, and the plan limit P_L) to limit the contact area of these structures in the three-dimensional space. Using the global coordinates of the reference points of the plan and sphere, the distance ($\mathbf{d}$) between the two structures can be determined using Eq. 23, while the associated relative velocity ($\dot{\mathbf{d}}$) is calculated using Eq. 24. Hence:

$$\mathbf{d} = \mathbf{r}_S - \mathbf{r}_P \quad (23)$$

$$\dot{\mathbf{d}} = \dot{\mathbf{r}}_S - \dot{\mathbf{r}}_P \quad (24)$$

The calculation of the contact force requires the decomposition of the distance and velocity vector on their normal and tangential components. For the distance vector this becomes:

$$\mathbf{d}_n = \left(\mathbf{d}^T \mathbf{n}_P \right) \frac{\mathbf{n}_P}{\left\| \mathbf{n}_P \right\|^2} \quad (25)$$

$$\mathbf{d}_t = \mathbf{d} - \mathbf{d}_n \quad (26)$$

Similar expressions are used for the calculation of the velocity components. Using the tangential and normal components of the distance vector, contact occurs when the two conditions, expressed in Eq. 27 and Eq. 28, are verified:

$$\left\| \mathbf{d}_n \right\| \le r \quad (27)$$

$$\left\| \mathbf{d}_t \right\| - r \le P_L \quad (28)$$

When contact occurs, the pseudo-penetration and pseudo-velocity values are computed using Eq. 29 and Eq. 30. The result is used in Eq. 20 to calculate the contact force module.

$$\delta = r - \left\| \mathbf{d}_n \right\| \quad (29)$$

$$\dot{\delta} = \left\| \dot{\mathbf{d}}_n \right\| \quad (30)$$

The contact force vector is then calculated using the contact force module and the unitary normal vector to the plan as expressed by Eq. 31. The force is applied at the contact point ($\mathbf{r}_{AP}$), which is calculated as the sum of the plan reference point and the tangential component of the distance vector, as indicated in Eq. 32. However, when the sphere center distance relatively to the plan reference point is greater than the plan limit the application will be given by Eq. 33.

$$\mathbf{F} = F_c \frac{\mathbf{n}_p}{\left\| \mathbf{n}_p \right\|} \quad (31)$$

$$\mathbf{r}_{AP} = \mathbf{r}_P + \mathbf{d}_t \quad (32)$$

$$\mathbf{r}_{AP} = \mathbf{r}_P + P_L \frac{\mathbf{d}_t}{\left\| \mathbf{d}_t \right\|} \quad (33)$$

The contact model also considers the action of a friction force F_F calculated according to the Coulomb friction model. The friction force is a resistive force

applied in the opposite direction of the tangential component of the velocity vector, as:

$$\mathbf{F}_F = -\mu F_c \frac{\dot{\mathbf{d}}_t}{\left\| \dot{\mathbf{d}}_t \right\|} \quad (34)$$

where μ is the friction coefficient and F_C the contact force calculated in Eq. 20.

The geometrical properties of the cervical ligaments in the lower and upper cervical ligaments are retrieved from the work of Ferreira [29], which adapted the points of the de Jager's cervical model [33]. In the lumbar spine, on the other hand, the data is computed using specific points in the vertebra as a reference (Figure 7) [51,52,53,54]. These studies are used in both regions to obtain the reference points and orientation of the contacts between the articular facets and the spinous processes. Notice that the upper cervical contacts geometry is retrieved from the work of de Jager [33].

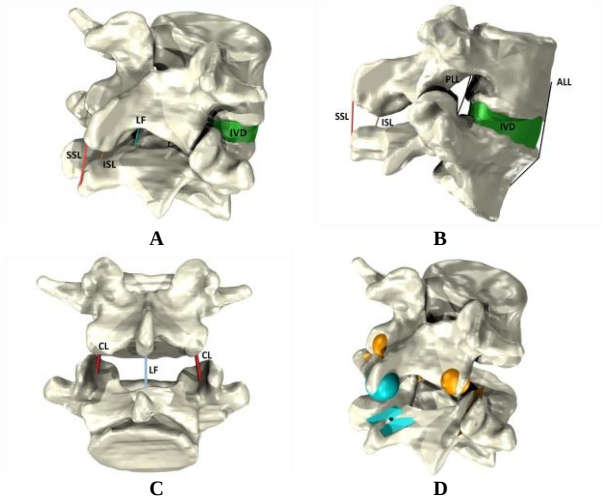

Figure 7 – Ligaments and contacts modelled in the multibody model of the spine: **A** – Interspinous and supraspinous ligaments; **B** – Anterior and posterior longitudinal ligaments; **C** – Capsular ligaments and ligamentum flavum; **D –** Articular facets (orange) and spinous process (blue) contacts.

With respect to the material properties, the stiffness and transition strains of the ligaments are retrieved from the work of Yoganadan et al. [55] (cervical spine), and from the work of Pintar et al. [56] and Chazal et al. [43] (lumbar spine). Notice that the material properties for the upper cervical ligaments are retrieved from the work of Ferreira [29], which adopted the approximation of van der Horst [48] and Meertens [57]. Moreover, the damping coefficients are retrieved from van der Horst [48] for the cervical spine and adopted for the lumbar ligaments and from Meertens [57] for the transverse ligament and tectorial membrane. The current spine model exhibits pretension, which is introduced in the ligaments (1.8 N and 3.0 N to the anterior and posterior longitudinal ligament [58,59], respectively, and 18.0 N [60] to the ligamentum flavum).

Relatively to the sphere-plan contacts, the relative stiffness between contact pairs is retrieved from the work of van der Horst [48] (K = 5862000 N/m), the nonlinearity parameter is considered equal to 1.5, and the restitution coefficient is retrieved from the work of Burgin and Aspden [61] (e = 0.476). Regarding the friction force, facet joints and spinous processes contacts are considered to be frictionless and therefore, in this work, the friction coefficient is set to zero.

2.4 The Finite Element Models of the Intervertebral Disc and Fixation Plate

The intervertebral disc is the most critical component in most of the finite element models of the spine due to its complex macro and microstructure and, consequently, its complex mechanical behaviour [62]. In the current work, two intervertebral discs finite element models for each region of the spine are developed. In the cervical spine, the IVD developed correspond to the C5-C6 and C6-C7, while, for the lumbar spine, correspond to the L3-L4 and L4-L5. These intervertebral joints present the intervertebral discs most susceptible to injury as reported by Tanaka et al. [63], which verified that a total of 75% of the patients analyzed presented prolapsed discs at C5-C6 or C6-C7 spine levels, and by Panjabi et al. [3] and Battiè et al. [64], which verified that the lumbar spine levels, L4-L5 and L5-S1, are the most susceptible since these levels bear the highest loads and undergo the most motion in the spine.

The IVDs are simulated as viscoelastic models comprising the annulus, the quasi-incompressible hydrostatic nucleus [65,66] and endplates, being symmetric relatively to the sagittal plan. The annulus matrix is reinforced by a network of collagen fibers modelled as tension only rebar elements, accounting for the radial variation in their inclination and stiffness.

The annulus fibrosus and nucleus pulposus geometry is obtained using software developed for the purpose and a cross-sectional image of the intervertebral disc. Notice that the nucleus geometry is obtained from the annulus geometry using the cross-sectional ratio between the nucleus and annulus area (Yoganandan et al. [45] for the cervical spine – 38 % and 58.2 % for the C5-C6 and C6-C7 IVD, respectively; and the O'Connell et al. [67] for the lumbar spine – 27.7 % for both lumbar IVDs). Finally, the interpolated points are converted from pixels to milimeters using two parametrization measurements: the intervertebral disc mean width and depth (retrieved from the work of Panjabi et al. [52, 68]). On the other hand, the height of the intervertebral disc is given by the mean height of the posterior and anterior measurements made by Nissan and Gilad [51], and the height retrieved from the work of de Jager [33], for the lumbar and cervical spine, respectively. The nucleus and annulus are modelled as viscoelastic materials, whose values are adapted from the studies of Wang et al. [69,70] for the lumbar spine, and Esat and Acar [27] for the cervical spine.

The collagen fibers are modelled as rebar elements, which are incorporated into surface sections (in order to not introduce additional stiffness to the annulus ground matrix besides that of the collagen fibers) that simulate the laminate structure of the annulus. To define the geometry of the rebar elements it is necessary to define their cross-sectional area (A), their angle of inclination and their spacing (s) between the fibers for each lamella, whose values are derived from the experimental data of Marchand and Ahmed [71]. The current intervertebral

disc models (Figure 8) do not have the 20 lamellae of the in vivo annulus, instead 8 lamellae are adopted for the FEM (as in the work of Little [72]). As such, the geometrical parameters are adapted to translate the mechanical properties of the in vivo set to the modelling set by assuming that the fiber bundles are elliptical and their width is 59% of the lamellae thickness.

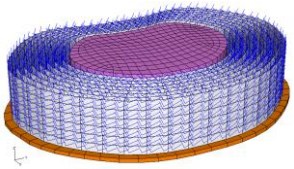

Figure 8 – Intervertebral disc model: endplate, annulus reinforced with collagen fibers and nucleus.

The fiber bundles are positioned at the center of each lamella in the radial direction, being spaced between them within the lamellae by 0.23 mm [71]. Furthermore, to define the fiber inclination it is necessary to establish a cylindrical local coordinate axis. The values for the fiber inclination vary with the position of the lamellae as well as its material properties. More specifically, the collagen fibers are modelled using linear elastic isotropic materials (retrieved from the work of Little [72]), which vary in order to the stiffness in the innermost layer is 65% of the stiffness in the outer layer [73]. Once defined the material and geometrical properties of the rebar elements, they are embedded into the continuum annulus fibrosus elements.

The cervical and lumbar IVD models are optimized relatively to their mesh and integrator used in order to obtain acceptable time analysis. As such, the following analyses are performed using the Direct Quasi-Newton method and assuming eight layers of elements in height. A further improvement includes the removal of the endplate in order to reduce the time analysis by 64% and due to its influence on the mechanical behaviour of the intervertebral disc (this situation is also verified in other studies [62]).

The intervertebral discs modelled in finite element are validated for several loading situations using experimental or other finite element studies. Namely, the lumbar spine are validated in compression (500 N simulating the torso weight plus 70 kPa pretension) and flexion (applying several rotations to the upper reference point of the IVD) using the studies of Markolf and Morris [74], Brown et al. [75], Shirazi-Adl et al. [76], Virgin [77],Schmidt et al. [78] and Little [72] presenting good results at exception of the higher rotation values, besides it is between the values of Shirazi-Adl et al. [79] and Little [72] (Table 1).

Prescribed Motion (deg)	Model (N.m)	Shirazi-Adl et al. (N.m)	Schmidt et al. (N.m/deg)	Little (N.m)
5.89	15.74	15.50	-	8.60
5.93	15.84	15.50	-	8.70
6.50	17.37	20.00	-	9.70
12.00	32.06	60.00	-	22.14
6.60	2.67 N.m/deg	-	1.80	2.10 N.m/deg

Table 1 – Prescribed flexion to the L4-L5 IVD finite element model and corresponding results, compared with the data from [72, 78, 79].

The cervical IVD, on the other hand, is compared to the experimental data of Moroney et al. [80], which subjected the C5-C6 motion segment to several moments or loads and a compressive load of 49 N corresponding to the head weight. According to the validation results it can be concluded that the IVD can predict accurately its biomechanics to compression, posterior shear and axial rotation (Table 2). Nonetheless, the model described is to too stiff in flexion and too lose in lateral bending and extension, which can be due to the parallel initial configuration assumed for the upper and lower surfaces of the intervertebral disc (may affect the behaviour of the collagen network whose action is only activated in tension).

Load Case	Load Applied	Moroney et al.	With Endplate	Without Endplate
Compression (mm)	73.6 N	-0.200	-0.208	-0.199
Ant. Shear (mm)	15.7 N	-0.400	-0.505	-0.463
Post. Shear (mm)	15.7 N	0.470	0.515	0.470
Lat. Shear (mm)	15.7 N	-0.290	-0.332	-0.307
Flexion (deg)	1.6 N.m	7.020	6.188	6.045
Extension (deg)	1.6 N.m	-4.800	-6.532	-6.366
Lat. Bending (deg)	1.6 N.m	-5.410	-6.131	-5.930
CCW Torsion (deg)	1.6 N.m	4.180	4.214	4.148

Table 2 – Time analysis with and without the endplate for several loading cases and comparison with the data from Moroney et al [80].

The C6-C7 cervical intervertebral disc is modeled using the same material properties, varying only its geometrical properties. As such, it is assumed that the behavior of this disc is similar to that of the C5-C6 and therefore it provides a reasonable data to conclude that the FE model for this spine level is acceptable. Similar reason is assumed for the validation of the L3-L4 IVD.

Besides the emphasis in this work is the finite element models of the intervertebral discs, the majority of the IVDs in the current work are represented as six DOF linear viscoelastic bushing elements. A comprehensive description of this type of elements is described in the work of van der Horst [48] and Ferreira [29].

A model of the fixation plate is developed with the objective of reproducing the environment in the vicinity of the intervertebral fusion and to analyze how the stresses distribute on this structure. The finite element model of the fixation plate is obtained from the work of Fernandes [81] and consists of the fixation plate and the corresponding screws, which are responsible to connect the plate to the vertebrae. The screws and the plate are assumed to be of titanium. On the other hand, the finite element models of the intervertebral disc substitutes are rectangular structures that are inserted into the intervertebral space, and therefore their geometrical properties are derived from the IVD, being their height assumed to be equal to that of the IVD and its width and depth assumed to be 90% of those from the IVD, being the thickness of the cage implant 14.3% of the disc substitute width (according to the width and thickness of the cage implant used by Chen et al. [82,83]). The material properties are derived from the work of Guan et al. [84] and Natarajan et al. [85], which define the material properties of the bone graft as E = 100 MPa, of the porous tantalum as E = 1570 MPa, and of the tricortical iliac crest bone graft as E = 3500 MPa, while the cage implant is assumed to be made of polyetheretherketone (PEEK) whose Young modulus is retrieved from the work of Chen et al. [83] and is equal to 3.6 GPa.

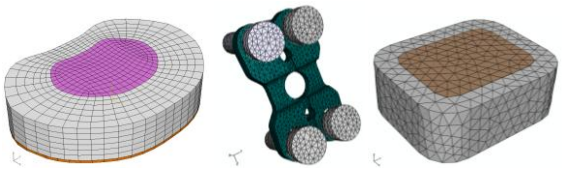

A **B** **C**

Figure 9 – Intervertebral disc (**A**), Fixation plate (**B**) and intervertebral disc substitute **(C)** model.

In order to model the intervertebral discs, it is necessary to define the respective reference points. The reference points used in the definition of each element are defined as the geometrical center of the lower and upper endplate of a given IVD, which is assumed to be, approximately, the geometrical center of the lower vertebral body's surface of a given vertebra and the upper surface of the subsequent vertebra, respectively. The initial translational and angular offsets are obtained considering the initial configuration of the spine model. Furthermore, the initial inclination is given in Bryant angles for bushing elements, while it is given in Euler angles for the co-simulation module.

The material properties of the cervical intervertebral discs simulated using bushing elements are obtained from Ferreira [29], which adapted the properties reported by van der Horst [48]. On the other hand, for the lumbar spine, the material properties are derived from the studies of Markolf [86], Virgin [77], Hirsch and Nachemson [87], Brown et al. [75] and Eberlein et al. [88].

3. Results

The cervical and lumbar spine models described are validated against values from several studies in order to determine the capabilities of each one to the several loading situations. The improved cervical spine model is validated for extension and flexion with the experimental data of Wheeldon et al. [89], Camacho et al. [90] (Table 3), Nightingale et al. [91,92], and Goël et al. [93]. The cervical spine model present a high stiffness to flexion and a low stiffness to extension, which translates to a good correlation of the model values for extension at small loads and a good correlation for flexion at relatively high loads. This is a consequence of the constant stiffness properties of the spinal structures that confer the spine with the same resistance (disregarding the velocity dependent component of their constitutive equations). Nonetheless, the presence of the contacts between the spinous processes is an improvement of the cervical spine model limiting the extension movements to a maximum value.

Spine Level	- 1.0 N.m		1.0 N.m	
	Model	Camacho	Model	Camacho
C3-C2 (deg)	-6.53	-5.53	4.55	5.03
C4-C3 (deg)	-6.78	-4.38	4.45	5.13
C5-C4 (deg)	-5.77	-3.61	4.49	5.82
C6-C5 (deg)	-5.94	-4.58	4.81	5.09
C7-C6 (deg)	-4.02	-3.55	4.77	3.73

Table 3 – Model rotations for the lower cervical spine levels for extension and flexion, compared with the data from [90].

Moreover, the model of the lumbar spine is validated for extension, flexion, lateral bending and axial rotation using the experimental data of Eberlein et al. [88] (Table 4), which applied several moments at the top of the vertebra L2 being the vertebra S1 fixed. The lumbar spine presents a high stiffness to lateral bending and is too loose for extension and flexion, producing acceptable results for axial rotation.

Load Situation	4.0 N.m		8.0 N.m	
	Model	Eberlein	Model	Eberlein
Extension (deg)	-11.6	-9.6	-15.0	-13.9
Flexion (deg)	22.9	15.0	26.2	18.7
Lat. Bend. (deg)	3.6	16.1	8.5	21.1
Torsion (deg)	-6.8	-4.7	-10.7	-7.5

Table 4 – Model rotations for the lumbar spine for several loading situations, compared with the data from [88].

The validations of the functional spine units involving the finite element models (for the cervical and lumbar spine) exhibit a good correlation with the experimental results [80,94] (Table 5), displaying a gain of using the co-simulation between the domains of the finite element models and the mulibody system dynamics.

Load Situation	C5-C6		L4-L5	
	Model	Moroney	Model	Heuer
Flexion (deg)	3.26	5.55	6.86	7.14
Extension (deg)	5.28	3.52	3.60	4.92
Lat. Bending (deg)	10.66	4.71	5.43	6.12
Torsion (deg)	8.25	1.85	4.42	3.45

Table 5 – Model rotations for the C5-C6 and L4-L5 spine levels for several loading situations, compared with the data from [80, 94].

In order to evaluate the influence of intersomatic fusion in the adjacent levels, two common movements of the spine are simulated before and after the chirurgic procedure: the extension and flexion movements. The movements are originated by applying a moment of 1.5 N.m to the head and during a time interval of 400 ms.

Independently of the type of movement, it can be seen that intersomatic fusion reduces the movement in the spine level subjected to this procedure almost completely, more even if it is complemented with the introduction of a fixation plate. More specifically, in extension, the rotation is reduced by 96.38% when an intervertebral disc surrogate is used and is further limited by a factor of 98.51% with the fixation plate (Figure 10). In flexion, the movement restriction increases, being of 98.34% for the intervertebral disc grafts and 99.41% with the inclusion of the titanium plate.

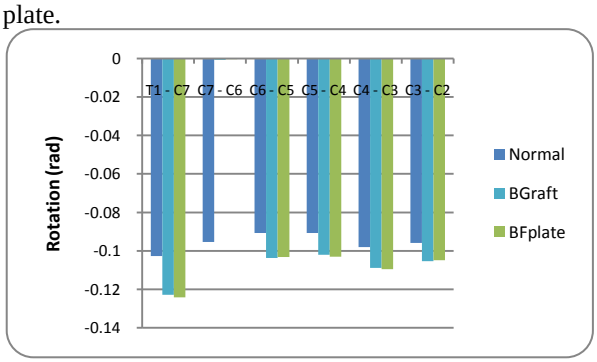

Figure 10 – Intervertebral rotation for the lower cervical spine levels in extension.

Furthermore, intersomatic fusion modifies the biomechanics of the spine levels in the vicinity of the fusioned area. Namely, it increases the rotational movement on the cervical spine levels in order to

compensate the loss of movement in C7-C6; nonetheless, the total motion of the cervical spine decreases relatively to the normal spine. Notice that the increase is not only verified in the adjacent levels, but also in non-adjacent spine levels. The rotational increase translates in higher stresses in the adjacent intervertebral disc (from 3.58 MPa for the normal cervical spine to 3.99 MPa for the cervical spine with bone graft and fixation plate), as can be seen in Figure 11 for flexion, which in a long-term physiological load can degenerate its structure. Similar observations for intersomatic fusion are found in the work of Ivanov et al. [95] for the lumbar spine. The fixation plate influence in these studies is not significantly noticed, as such, further analyses are necessary to determine its influence in the spine biomechanics.

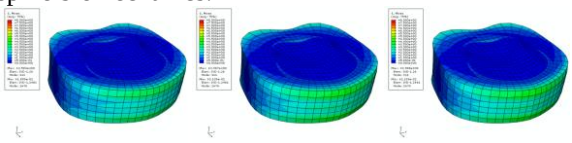

A **B** **C**

Figure 11 – Stress distribution in the C5-C6 intervertebral disc in flexion: normal cervical spine (**A**), cervical spine with a bone graft (**B**), and cervical spine with a bone graft and fixation plate (**C**).

Moreover, the single-level fusion not only affects the intervertebral discs but also the facet joints in extension. Namely, the load sharing by the facet joints increases as a result of an increase in the movement associated with each motion segment, which may affect the integrity of this structure and originate additional pathologies, as facet arthropathy. These results are in agreement with the results of Guan et al. [84] for the lumbar spine.

In the current work, several types of materials are studied in the cervical and lumbar spine. In the cervical spine, the bone graft is compared to the cancellous graft, while in the lumbar spine, these two graft materials are also compared to the porous tantalum graft. Observing the results, it can be concluded that higher elastic modulus translates in a higher restriction of the movement in the fusioned level and a greater rotational movement on the other spine levels (Figure 12).

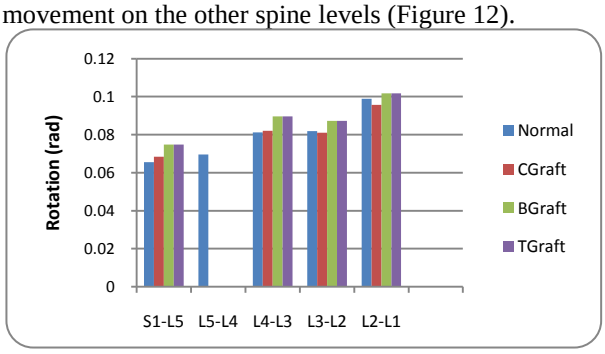

Figure 12 – Intervertebral rotation for the lumbar spine levels in flexion using several types of graft materials.

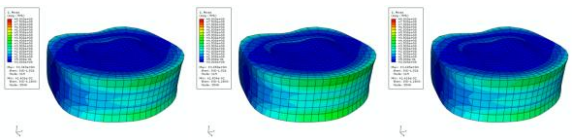

A **B** **C**

Figure 13 – Stress distribution in the C5-C6 intervertebral disc in extension: normal cervical spine (**A**), cervical spine with a bone graft (**B**), and cervical spine with a cancellous graft (**C**).

The forces exerted over the facet joints also vary with the type of material, being greater for the materials that are responsible for a greater motion in the motion segments near the one subjected to intersomatic fusion, i.e., with higher elastic modulus. As a consequence, the stresses induced in the adjacent intervertebral disc structure are higher for the cervical spine with bone graft (with a 14.51% increase) (Figure 13).

4. Conclusions and Future Developments

In the current work, a co-simulation module is applied in the study of the dynamic stress distributions on the IVD adjacent to the vertebral level that is engaged with a bone graft and, simultaneously, on the fixation plate that is placed along one cervical stage during the surgical intervention of intervertebral fusion. The combination of the two types of models (finite element models and multibody models) allows analyzing simultaneously, in an integrated way, the kinematics and the stress distribution on the structures of interest for any particular region of the vertebral column. This is extremely important from the clinical point of view as it will allow for the identification of the regions of the spine that, for a given movement, present the higher stresses and where the risk of injury is higher. Furthermore, it can be used in the future to develop or analyze different types of materials and geometrical designs for the orthopaedic implants. Nonetheless an effort has to be done to optimize the co-simulation process in order to turn it faster and more efficient. Additionally, there is a problem in the prescription of all degrees of freedom to the finite element models, since the convergence of the FE decreases. As such, a processing step of the loads and moments retrieved from the finite element models have to be created and executed in order to satisfy the equilibrium equations.

In order to study the stress distribution on the discs adjacent to a single-level intersomatic fusion, the movements of the spine are analyzed before and after the fusion with the bone graft and with or without the fixation plate. These analyses require the development and validation of the multibody models of the cervical and lumbar spine regions, as well as the finite element models of the IVD developed for the same spine regions. Namely, the cervical IVD can predict accurately its biomechanics to compression, posterior shear and axial rotation, being too stiff in flexion and too lose in lateral bending and extension. On the other hand, the lumbar disc exhibits moments that are within the values of Shirazi-Adl et al. [79] and Schmidt et al. [78] for small rotations. The multibody models of the spine regions present distinct results: the lumbar spine cannot show good correlation with the data of Eberlein et al. [88] for flexion and lateral bending, being capable of predicting acceptably for axial rotation while the cervical spine model present a high stiffness to flexion and a low stiffness to extension, which translates to a good correlation of the model values for extension at small loads and a good correlation for flexion at relatively high loads.

The single level intersomatic fusion determines alterations in the biomechanics not only of the motion segment it affects directly but also of the spine levels in

their vicinity. Namely, the motion of the level subjected to fusion is highly restricted by using only an intervertebral substitute or by complementing with the inclusion of a fixation plate, while the adjacent levels and the other spine levels near to the fusioned area exhibit an increase in their rotational movement (higher in the adjacent levels). The higher rotational movement implies higher stresses in the intervertebral disc and an increased load sharing by the facet joints. The higher loads experienced by these structures, posteriorly to fusion, may be responsible for their degeneration and, consequently, to spine refusion as reported by other researchers. Nonetheless, further analyses taking into account different loads and longer time analysis are necessary to reinforce these results.

Acknowledgements

The computational methodologies developed in the scope of this work unfold under the objectives of the FCT projects DACHOR – Multibody Dynamics and Control of Hybrid Active Orthoses (MIT-Pt/BS-HHMS/0042/2008) and PROPAFE - Design and Development of a Patello-Femoral Prosthesis (PTDC/EME-PME/67687/2006).

References

[1] Rouvière H., *Anatomie Humaine – Descriptive et Topographique: Tome II Tronc*, Masson et C^{ie}, 10th Edition, 1970.

[2] Ehlers W., Markert B., Karajan N., Acartürk A., *A Coupled FE Analysis of the Intervertebral Disc Based on a Multiphasic TPM Formulation*, in Proceedings of IUTAM Symposium on Mechanics of Biological Tissue, Editors Holzapfel G. A., Ogden R. W., Springer, pp. 373-386, 2005.

[3] White A. A., Panjabi M. M., *Clinical Biomechanics of the Spine*, Lippincott Williams & Wilkins, 2nd Edition, 1970.

[4] Best B. A., Guilak F., Setton L. A., Zhu W., Saed-Nejad F., Ratcliffe A., Weidenbaum M., Mow V. C., *Compressive Mechanical Properties of the Human Annulus Fibrosus and Their Relationship to Biomechanical Composition*, Spine, Vol. 19, No. 2, pp. 212-221, 1994.

[5] Costi J. J., Stokes I. A., Gardner-Morse M., Laible J. P., Scoffone H. M., Iatridis J. C., *Direct Measurement of the Intervertebral Disc Maximum Shear Strain in Six Degree of Freedom: Motions that Place Disc Tissue at Risk of Injury*, Journal of Biomechanics, Vol. 40, pp. 2457-2466, 2007.

[6] Skaggs D. L., Weidenbaum M., Iatridis J. C., Ratcliffe A., Mow V. C., *Regional Variation in Tensile Properties and Biochemical Composition of the Lumbar Annulus Fibrosus*, Spine, Vol. 19, No. 12, pp. 1310-1319, 1994.

[7] Harris R. I., Macnab I., *Structural Changes in the Lumbar Intervertebral Disc: Their Relationship to Low Back Pain and Sciatica*, The Journal of Bone and Joint Surgery, Vol. 36B, No. 2, pp. 304-322, 1954.

[8] Brown S. H. M., Gregory D. E., McGill S. M., *Vertebral Endplate Fractures as a Result of High Rate Pressure Loading in the Nucleus of the Young Adult Porcine Spine*, Journal of Biomechanics, Vol. 41, pp. 122-127, 2008.

[9] Cusick J. F., Yoganandan N., *Biomechanics of the Cervical Spine 4: Major Injuries*, Clinical Biomechanics, Vol. 17, pp. 1-20, 2002.

[10] Shirazi-Adl A., *Finite Element Simulation of Changes in the Fluid Content of Human Lumbar Discs: Mechanical and Clinical Implications*, Spine, Vol. 17, No. 2, pp. 206-212, 1992.

[11] Dvorak M., Pitzen T., Zhu O., Gordon J., Fisher C., Oxland T., *Anterior Cervical Plate Fixation: A Biomechanical Study to Evaluate the Effects of Plate Design, Endplate Preparation, and Bone Mineral Density*, Spine, Vol. 30, No. 3, pp. 294-301, 2005.

[12] Green P. W. B., *Anterior Cervical Fusion: A Review of 33 Patients with Cervical Disc Degeneration*, The Journal of Bone and Joint Surgery, Vol. 59B, No. 2, pp. 236-240, 1977.

[13] Hilibrand A. S., Balasubramanian K., Eichenbaum M., Thinnes J. H., Daffner S., Berta S., Albert T. J., Vaccaro A. R., Siegler S., *The Effect of Anterior Cervical Fusion on Neck Motion*, Spine, Vol. 31, No. 15, pp. 1688-1692, 2006.

[14] Lopez-Espina C. G., Amirouche F., Havalad V., *Multilevel Cervical Fusion and Its Effect on Disc Degeneration and Osteophyte Formation*, Spine, Vol. 31, No. 9, pp. 972-978, 2006.

[15] Skalli W., Robin S., Lavaste F., Dubousset J., *A Biomechanical Analysis of Short Segment Spinal Fixation Using a Three-Dimensional Geometric and Mechanical Model*, Spine, Vol. 18, No. 5, pp. 536-545, 1993.

[16] Gillet P., *The Fate of Adjacent Motion Segments after Lumbar Fusion*, Journal of Spinal Disorders and Techniques, Vol. 16, No. 4, pp. 338-345, 2003.

[17] Rao R. D., Wang M., McGrady L. H., Perlewitz T. J., Dacid K. S., *Does Anterior Plating of the Cervical Spine Predispose to Adjacent Segment Changes?*, Spine, Vol. 30, No. 24, pp. 2788-2792, 2005.

[18] Wang J., Ma Z.-D., Hulbert G. M., *A Gluing Algorithm for Distributed Simulation of Multibody Systems*, Nonlinear Dynamics, Vol. 34, pp. 159-188, 2003.

[19] Rauter F. G., Pombo J., Ambrósio J., Pereira M., *Multibody Modeling of Pantographs for Pantograph-Catenary Interaction*, in IUTAM Symposium On Multiscale Problems in Multibody System Contacts, Editor Eberhard P., pp. 205-226, Springer, 2007.

[20] Latham F., *A Study in Body Ballistics: Seat Ejection*, in Proceedings of the Royal Society of London, Vol. 147, pp. 121-139, 1957.

[21] Dooris A. P., Goël V. K., Grosland N. M., Gilbertson L. G., Wilder D. G., *Load Sharing Between Anterior and Posterior Elements in a Lumbar Motion Segment Implanted with an Artificial Disc*, Spine, Vol. 24, No. 6, pp. E122-E129, 2001.

[22] Goël V. K., Lim T.-H., Gwon J., Chen J.-Y., Winterbottom J. M., Park J. B., Weinstein N., Ahn J.-Y., *Effects of Rigidity of an Internal Fixation Device: A Comprehensive Biomechanical Investigation*, Spine, Vol. 16, No. 3, pp. S155-S161, 1991.

[23] Mizrahi J., Silva M. J., Keaveny T. M., Edwards W. T., Hayes W. C., *Finite Element Stress Analysis of the Normal and Osteoporotic Lumbar Vertebral Body*, Spine, Vol. 18, No. 14, pp. 2088-2096, 1993.

[24] Tschirhart C. E., Finkelstein J. A., Whyne C. M., *Biomechanics of Vertebral Level, Geometry, and Transcortical Tumors in the Metastatic Spine*, Journal of Biomechanics, Vol. 40, pp. 46-54, 2007.

[25] Esat V., Acar M., *A Multibody Human Spine Model for Dynamic Analysis in Conjunction with the FE Analysis of Spinal Parts*, in Proceedings of 1st Annual Injury Biomechanics Symposium, The Ohio State University, USA, 2005.

[26] Esat V., van Lopik D. W., Acar M., *Combined Multi-Body Dynamic and FE Models of Human Head and Neck*, in IUTAM Proceedings on Impact Biomechanics: from Fundamental Insights to Application, Editor Gilchrist M. D., pp. 91-100, Springer, 2005.

[27] Esat V., Acar M., *Viscoelastic Finite Element Analysis of the Cervical Intervertebral Discs in Conjuction with a Multi-Body Dynamic Model of the Human Head and Neck*, Proceedings of the Institution of Mechanical Engineers, Part H: Journal of Engineering in Medicine, pp. 249-262, 2009.

[28] Silva M. T., *Human Motion Analysis Using Multibody Dynamics and Optimization Tools*, PhD. Thesis Instituto Superior Técnico – Technical University of Lisbon, Lisbon, 2003.
[29] Ferreira A., *Multibody Model of the Cervical Spine and Head for the Simulation of Traumatic and Degenerative Disorders*, M. Sc. Thesis Instituto Superior Técnico – Technical University of Lisbon, Lisbon, 2008.
[30] van Lopik D. W., Acar M., *Dynamic Verification of a Multibody Computational Model of Human Head and Neck for Frontal, Lateral and Rear Impacts*, Proceedings of the Institution of Mechanical Engineers, Part K: Journal of Multibody Dynamics, Vol. 221, No. 2, pp. 199-217, 2007.
[31] Stokes I. A. F., Gardner-Morse M., *Quantitative Anatomy of the Lumbar Musculature*, Journal of Biomechanics, Vol. 32, pp. 311-316, 1999.
[32] Gangnet N., Dumas R., Pomero V., Mitulescu A., Skalli W., Vital J.-M., *Three-Dimensional Spinal and Pelvic Alignment in an Asymptomatic Population*, Spine, Vol. 31, No. 15, pp. E507-E512, 2006.
[33] de Jager M., *Mathematical Head-Neck Models for Acceleration Impacts*, Technische Universiteit Eindhoven – University of Technology, Eindhoven, 2000.
[34] Laananen D., *Computer Simulation of an Aircraft Seat and Occupant in a Crash Environment – Program SOM-LA / SOM-TA User Manual*, DOT/FAA/CT-90/4, US Department of Transportation, Federal Aviation Administration, 1991.
[35] Ambrósio J. A. C., *Multibody Dynamics: Bridging for Multidisciplinary Applications*, in Mechanics of the 21st Century, Editors Gutkowski W., Kowalewski, Springer, pp. 61-88, 2005.
[36] Monteiro N., Folgado J., Silva M., Melancia J., *Analysis of the Intervertebral Discs Using a Finite Element and Multibody Dynamics Approach*, 8th World Congress on Computational Mechanics (WCCM8), 5th European Congress on Computational Methods in Applied Sciences and Engineering (ECCOMAS 2008), Venice, Italy, June 30 – July 5, 2008.
[37] Monteiro N., Folgado J., Silva M., Melancia J., *Co-Simulação de Sistemas Multicorpo com Modelos de Elementos Finitos: Aplicação à Análise de Tensões nos Discos Intervertebrais*, 3º Congresso Nacional de Biomecânica, Bragança, 2009.
[38] Monteiro N., Folgado J., Silva M., Melancia J., *Dynamic Stress Distribution on a Multilevel Cervical Fusion Using a MSD/FE Co-Simulation Approach*, Proceedings of Multibody Dynamics 2009 An ECCOMAS Thematic Conference, Warsaw, Poland, June 29 – July 2, 2009.
[39] Monteiro N., Folgado J., Silva M., Melancia J., *A New Approach to Analyze the Stress Distribution on a Multilevel Cervical/Lumbar Intersomatic Fusion*, Proceedings of ESMC2009, 7th EUROMECH Solid Mechanics Conference, Lisbon, Portugal, September 7 – 11 2009.
[40] Nikravesh P., *Computer-Aided Analysis of Mechanical Systems*, Prentice-Hall, Englewood Cliffs, New Jersey, 1988.
[41] Panjabi M. M., Oxland T. R., Parks E. H., *Quantitative Anatomy of Cervical Spine Ligaments. Part I: Upper Cervical Spine*, Journal of Spinal Disorders and Techniques, Vol. 4, Nº 3, pp. 270-276, 1991.
[42] Sharma M., Langrana N. A., Rodriguez J., *Role of Ligaments and Facets in Lumbar Spinal Stability*, Spine, Vol. 20, No. 8, pp. 887-900, 1995.
[43] Chazal J., Tanguy A., Bourges M., Gaurel G., Escande G., Guillot M., Vanneuville G., *Biomechanical Properties of Spinal Ligaments and a Histological Study of the Supraspinal Ligament in Traction*, Journal of Biomechanics, Vol. 18, No. 3, pp. 167-176, 1985.
[44] Panjabi M. M., *The Stabilizing System of the Spine – Part II: Neutral Zone and Instability Hypothesis*, Journal of Spinal Disorders and Techniques, Vol. 5, pp. 390-396, 1992.
[45] Yoganandan N., Kumaresan S., Pintar F. A., *Biomechanics of the Cervical Spine Part 2: Cervical Spine Soft Tissue Responses and Biomechanical Modeling*, Clinical Biomechanics, Vol. 16, pp. 1-27, 2001.
[46] Martin R. B., Burr D. B., Sharkey N. A., *Skeletal Tissue Mechanics*, Springer, United States of America, 2004.
[47] Wisman J., *A Three-Dimensional Mathematical Model of the Human Knee Joint*, PhD. Thesis, Technische Hogenschool Eindhoven, 1980.
[48] van der Horst M., *Human Head Neck Response in Frontal, Lateral and Rear End Impact Loading*, Technisch Universiteit Eindhoven – University of Technology, Eindhoven, 2002.
[49] Ambrósio J. A., Silva M., *Multibody Dynamics Approaches for Biomechanical Modeling in Human Impact Application*, in IUTAM Proceedings on Impact Biomechanics: From Fundamental Insights to Applications, Editor Gilchrist M. D., Springer, pp. 61-80, 2005.
[50] Hertz H., *On the Contact of Solids – On the Contact of Rigid Elastic Solids and on Hardness*, Miscellaneous Papers, MacMillan and Co. Ltd., London, pp. 146-183, 1896.
[51] Nissan M., Gilad I., *The Cervical and Lumbar Vertebrae - An Anthropometric Model*, Engineering in Medicine, Vol. 13, No. 3, pp. 111-114, 1984.
[52] Panjabi M. M., Duranceau J., Goel V., Oxland T., Takata K., *Cervical Human Vertebrae: Quantitative Three-Dimensional Anatomy of the Middle and Lower Regions*, Spine, Vol. 16, No. 8, pp. 861-869, 1991.
[53] Panjabi M. M., Oxland T., Takata K., Goël V., Duranceau J., Krag M., *Articular Facets of the Human Spine: Quantitative Three-Dimensional Anatomy*, Spine, Vol. 18, No. 10, pp. 1298-1310, 1993.
[54] Xu R., Burgar A., Ebraheim N. A., Yeasting R. A., *The Quantitative Anatomy of the Laminas of the Spine*, Spine, Vol. 24, No. 2, pp. 107-113, 1999.
[55] Yoganandan N., Kumaresan S., Pintar F. A., *Geometrical and Mechanical Properties of Human Cervical Spine Ligaments*, Journal of Biomechanical Engineering, Vol. 122, pp. 623-629, 2000.
[56] Pintar F. A., Yoganandan N., Myers T., Elhagediab A., Sances A. Jr., *Biomechanical Properties of Human Lumbar Spine Ligaments*, Journal of Biomechanics, Vol. 25, No. 11,, pp. 1351-1356, 1992.
[57] Meertens W., *Mathematical Modelling of the Upper Cervical Spine with MADYMO*, Final Thesis, Eindhoven University of Technology, 1995.
[58] Hukins D. W. L., Kirby M. C., Sikoryn T. A., Aspden R. M., Cox A. J., *Comparison of Structure, Mechanical Properties, and Functions of Lumbar Spinal Ligaments*, Spine, Vol. 15, No. 8, pp. 787-795, 1990.
[59] Tkaczuk H., *Tensile Properties of Human Lumbar Longitudinal Ligaments*, Acta Orthopaedica Scandinava, Vol. 115 (Supplement), 1968.
[60] Nachemson A., Evans J., *Some Mechanical Properties of the Third Lumbar Inter-Laminar Ligament (Ligamentum Flavum)*, Journal of Biomechanics, Vol. 1, No. 211, 1968.
[61] Burgin L. V., Aspden R. M., *Impact Testing to Determine the Mechanical Properties of Articular Cartilage in Isolation and on Bone*, Journal of Material Science: Materials in Medicine, Vol. 19, pp. 703-711, 2008.
[62] Fagan M. J., Julian S., Siddall D. J., Mohsen A. M., *Patient-Specific Spine Models. Part 1: Finite Element Analysis of the Lumbar Intervertebral Disc – A Material Sensitivity Study*, Proceedings of Institution of Mechanical Engineers, Part H: Journal of Engineering in Medicine, Vol. 216, pp. 299-314, 2002.

[63] Tanaka N., Fujimoto Y., An H. S., Ikuta Y., Yasuda M., *The Anatomic Relation Among the Nerve Roots, Intervertebral Foramina, and Intervertebral Disc of the Cervical Spine*, Spine, Vol. 25, No. 3, pp. 286-291, 2000.
[64] Battié M. C., Videman T., Parent E., *Lumbar Disc Degeneration: Epidemiology and Genetic Influences*, Spine, Vol. 29, No. 23, pp. 2679-2690, 2004.
[65] Bogduk N., *Clinical Anatomy of the Lumbar Spine and Sacrum*, Churchill Livingstone, New York, 1997.
[66] Nachemson A., *Lumbar Intradiscal Pressure: Experimental Studies on Postmortem Material*, Acta Orthopaedica Scandinava, Vol. 43, pp. 9-104, 1960.
[67] O'Connell G., Vresilovic E., Elliott D., *Comparison of Animals Used in Disc Research to Human Lumbar Disc Geometry*, Spine, Vol. 32, No. 3, pp. 328-333, 2007.
[68] Panjabi M. M., Goel V., Oxland T., Takata K., Duranceau J., Krag M., Prince M., *Human Lumbar Vertebrae: Quantitative Three-Dimensional Anatomy*, Spine, Vol. 17, No. 3, pp. 299-306, 1992.
[69] Wang J. L., Parnianpour M., Shirazi-Adl A., Engin A. E., Li S., Patwardhan A., *Development and Validation of a Viscoelastic Finite Element Model of an L2-L3 Motion Segment*, Theoretical and Applied Fracture Mechanics, Vol. 28, pp. 81-93, 1997.
[70] Wang J. L., Parnianpour M., Shirazi-Adl A., Engin A. E., *Viscoelastic Finite Element Analysis of a Lumbar Motion Segment in Combined Compression and Sagittal Flexion*, Spine, Vol. 25, No. 3, pp. 310-318, 2000.
[71] Marchand F., Ahmed A., *Investigation of the Laminate Structure of Lumbar Disc Annulus Fibrosus*, Spine, Vol. 15, No. 5, pp. 402-410, 1990.
[72] Little J. P., *Finite Element Modeling of Anular Lesions in the Lumbar Intervertebral Disc*, PhD. Thesis, Queensland University of Technology, 2004.
[73] Eyre D., Muir H., *Types I and II Collagens in Intervertebral Disc: Interchanging Radial Distributions in Annulus Fibrosus*, Biochemistry Journal, Vol. 157, No. 1, pp. 267-270, 1976.
[74] Markolf K. L., Morris J. M., *The Structural Components of the Intervertebral Disc: A Study of their Contributions to the Ability of the Disc to Withstand Compressive Forces*, Journal of Bone and Joint Surgery, Vol. 56, pp. 675-687, 1974.
[75] Brown T., Hanson R., Yorra A., *Some Mechanical Tests on the Lumbo-Sacral Spine with Particular Reference to the Intervertebral Discs*, Journal of Bone and Joint Surgery, Vol. 39A, pp.1135-1164, 1957.
[76] Shirazi-Adl A., Shrivastava S. C., Ahmed A. M., *Stress Analysis in the Lumbar Disc Body Unit in Compression*, Spine, Vol. 9, pp. 120-134, 1984.
[77] Virgin W., *Experimental Investigations into Physical Properties of Intervertebral Disc*, Journal of Bone and Joint Surgery, Vol. 33B, pp. 607, 1951.
[78] Schmidt T. A., An H. S., Lim T, Nowicki B. H., Haughton V. M., *The Stiffness of Lumbar Spinal Motion Segments with a High-Intensity Zone in the Anulus Fibrosus*, Spine, Vol. 23, No. 20, pp. 2167-2173, 1998.
[79] Shirazi-Adl A., Ahmed A. M., Shrivastava S. C., *A Finite Element Study of a Lumbar Motion Segment Subjected to Pure Sagittal Plane Moments*, Journal of Biomechanics, Vol. 19, No. 4, pp. 331-350, 1986.
[80] Moroney S. P., Schultz A. B., Miller J. A. A., Andersson G. B. J., *Load-Displacement Properties of Lower Cervical Spine Motion Segments*, Journal of Biomechanics, Vol. 21, pp. 767-779, 1988.
[81] Fernandes P., *Modelação e Análise da Fusão Intersomática Cervical*, M. Sc. Thesis Instituto Superior Técnico – Technical University of Lisbon, Lisbon, Portugal, 2008.
[82] Chen J.-F., Wu C.-T., Lee S.-C., Lee S.-T., *Use of a Polymethylmethacrylate Cervical Cage in the Treatment of Single-Level Cervical Disc Disease*, Journal of Neurosurgery Spine, Vol. 3, pp. 24-28, 2005.
[83] Chen J.-F., Lee S.-T., *The Polymethyl Methacrylate Cervical Cage for Treatment of Cervical Disc Disease. Part III: Biomechanical Properties*, Surgical Neurology, Vol. 66, pp. 367-370, 2006.
[84] Guan Y., Yoganandan N., Maiman D. J., Pintar F. A., *Internal and External Responses of Anterior Lumbar / Lumbosacral Fusion: Nonlinear Finite Element Analysis*, Journal of Spinal Disorders and Techniques, Vol. 21, No. 4, 2008.
[85] Natarajan R. N., Chen B. H., An H. S., Andersson G. B. J., *Anterior Cervical Fusion: A Finite Element Model Study on the Motion Segment Stability Including the Effect of Osteoporosis*, Spine, Vol. 25, No. 8, pp. 955-961, 2000.
[86] Markolf K. L., *Stiffness and Damping Characteristics of the Thoracic-Lumbar Spine*, in Proceedings of Workshop on Bioengineering Approaches to the Problems of the Spine, NIH, September, 1970.
[87] Hirsch C., Nachemson A., *A New Observation on the Mechanical Behaviour of Lumbar Discs*, Acta Orthopaedica Scandinava, Vol. 23, pp. 254, 1954.
[88] Eberlein R., Holzapfel G. A., Fröhlich M., *Multi-Segment Finite Element Analysis of the Human Lumbar Spine Including the Heterogeneity of the Annulus Fibrosus*, Computational Mechanics, Vol. 34, pp. 147-163, 2004.
[89] Wheeldon J. A., Pintar F. A., Knowles S., Yoganandan N., *Experimental Flexion/Extension Data Corridors for Validation of Finite Element Models of the Young, Normal Cervical Spine*, Journal of Biomechanics, Vol. 39, pp. 375-380, 2004.
[90] Camacho D. L., Nightingale R. W., Robinette J. J., Vanguri S. K., Coates D. J., Myers B. S., *Experimental Flexibility Measurements for the Development of a Computational Head-Neck Model Validated for a Near-Vertex Head Impact*, Society of Automotive Engineers, Paper No. 973345, 1997.
[91] Nightingale R. W., Winkelstein B. A., Knaub K. E., Richardson W. J., Luck J. F., Myers B. S., *Comparative Strengths and Structural Properties of the Upper and Lower Cervical Spine in Flexion and Extension*, Journal of Biomechanics, Vol. 35, pp. 725-732, 2002.
[92] Nightingale R. W., Chancey V. C., Ottaviano D., Luck J. F., Tran L., Prange H., Myers B. S., *Flexion and Extension Structural Properties and Strengths for Male Cervical Spine Segments*, Journal of Biomechanics, Vol. 40, pp. 535-542, 2007.
[93] Goël V., Clark C., Gallaes K., King Liu Y., *Moment-Rotation Relationships of the Ligamentous Occipito-Axial Complex*, Journal of Biomechanics, Vol. 21, No. 8, pp. 673-680, 1988.
[94] Heuer F., Schmidt H., Klezl Z., Claes L., Wike H.-J., *Stepwise Reduction of Functional Spinal Structures Increase Range of Motion and Change Lordosis Angle*, Journal of Biomechanics, Vol. 40, pp. 271-280, 2007.
[95] Ivanov A. A., Kiapour A., Ebraheim N. A., Goël V., *Lumbar Fusion Leads to Increases in Angular Motion and Stress Across Sacroiliac Joint*, Spine, Vol. 34, No. 5, pp. E162-E169, 2009.